

Sustainable Electrosynthesis of *N,N*-Dimethylformamide via Relay Catalysis on Synergistic Active Sites

Weihang Li, Haoyang Jiang, Xiang Zhang, Bo Lei, Le Li, Haoshen Zhou,* and Miao Zhong*



Cite This: *J. Am. Chem. Soc.* 2024, 146, 21968–21976



Read Online

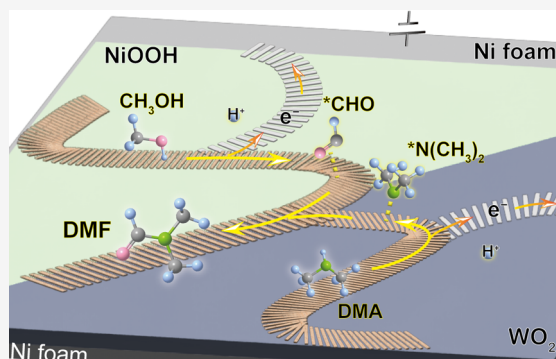
ACCESS |

Metrics & More

Article Recommendations

Supporting Information

ABSTRACT: Electrified synthesis of high-value organonitrogen chemicals from low-cost carbon- and nitrogen-based feedstocks offers an economically and environmentally appealing alternative to traditional thermocatalytic methods. However, the intricate electrochemical reactions at electrode surfaces pose significant challenges in controlling selectivity and activity, especially for producing complex substances such as *N,N*-dimethylformamide (DMF). Herein, we tackle this challenge by developing relay catalysis for efficient DMF production using a composite WO_2 –NiOOH/Ni catalyst with two distinctive active sites. Specifically, WO_2 selectively promotes dimethylamine (DMA) electrooxidation to produce strongly surface-bound $(\text{CH}_3)_2\text{N}^*$, while nearby NiOOH facilitates methanol electrooxidation to yield more weakly bound ${}^*\text{CHO}$. The disparity in binding energetics of the key C- and N-intermediates expedites C–N coupling at the WO_2 –NiOOH interface. *In situ* infrared spectroscopy with isotope-labeling experiments, quasi-*in situ* electron paramagnetic resonance trapping experiments, and electrochemical operating experiments revealed the C–N coupling mechanism and enhanced DMF-synthesis selectivity and activity. *In situ* X-ray absorption spectroscopy (XAS) and postreaction transmission electron microscopy (TEM) studies verified the stability of WO_2 –NiOOH/Ni during extended electrochemical operation. A Faradaic efficiency of ~50% and a production rate of $438 \mu\text{mol cm}^{-2} \text{ h}^{-1}$ were achieved at an industrially relevant current density of 100 mA cm^{-2} over an 80 h DMF production period. This study introduces a new paradigm for developing electrothermo relay catalysis for the sustainable and efficient synthesis of valuable organic chemicals with industrial potential.



INTRODUCTION

N,N-dimethylformamide (DMF) plays a pivotal role as a chemical feedstock and is widely used to manufacture synthetic fibers, pharmaceuticals, polyurethane, and electronic devices.^{1–3} The annual global market demand for DMF exceeds USD 20 billion and is projected to grow at a compound annual growth rate of 3.2% by 2027.⁴ Traditional industrial DMF-synthesis processes (Figure 1a) rely on energy-intensive thermocatalytic methods that use fossil-fuel-derived carbon monoxide and dimethylamine (DMA) as reactants at elevated pressures (2–10 MPa) and temperatures (80–100 °C).^{5,6} These harsh conditions necessitate complicated reaction setups⁷ that result in substantial energy consumption and notable CO₂ emissions.

Electrified synthesis of DMF using renewable electricity offers a promising solution to the above-mentioned challenges. Electrocatalysis with its simpler device configurations and rapid reactions under mild conditions leverages clean energy sources to produce DMF, contributing to more sustainable and decarbonized technology.^{8–11} Recent research has explored the electrochemical coreduction of CO₂ and N₂/NO_x for the synthesis of urea^{12–16} and methylamine;¹⁷ however, producing more complex organic compounds, such as DMF, directly from the reduction of CO₂ and N₂/NO_x faces considerable energetic

and chemical hurdles. Specifically, how to harness an electric field to drive the electrode reactions and elucidate the electrochemical and catalytic mechanisms involved in this complicated electrosynthetic process remains unexplored. Furthermore, in the electrochemical reduction configuration, the anodic reaction of oxygen evolution reaction (OER) has low economic value and high overpotential, resulting in substantial energy loss.¹⁸ To address these challenges, we explored producing DMF via anodic oxidation, transforming electrocatalysis into a viable route for DMF production. This approach is accompanied by environmentally benign cathodic hydrogen evolution (HER)¹⁹ or CO₂ reduction reactions,^{20–22} resulting in products of higher economic value at both electrodes. The challenge here lies in producing DMF selectively and efficiently using cost-effective feedstocks. These reactants should readily undergo oxidation with minimal

Received: May 25, 2024

Revised: July 16, 2024

Accepted: July 17, 2024

Published: July 25, 2024



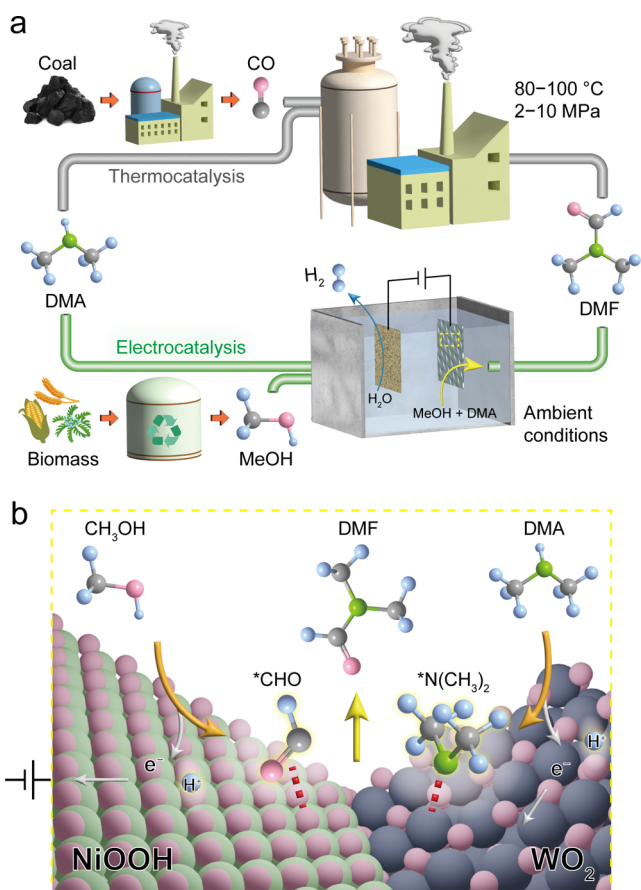


Figure 1. (a) Illustration of the current industrial route and proposed electrooxidation route under $\text{WO}_2\text{--NiOOH}$ electrocatalysis for the synthesis of N,N -dimethylformamide (DMF). (b) Chemical framework for relay catalysis involving selective anodic oxidation of methanol (CH_3OH) and dimethylamine (DMA) on NiOOH and WO_2 surfaces, respectively, and fast thermocatalytic C–N coupling at the $\text{WO}_2\text{--NiOOH}$ interfaces for DMF production.

energy barriers but not so readily that they self-oxidize to their respective oxidation byproducts prior to C–N coupling. In addition, the oxidation reaction should preferably occur in the liquid/solid phase, thereby eliminating mass-transfer issues and enabling industrial-level current densities.²³

Herein, we present relay catalysis that leverages an electric field to produce DMF by selectively co-oxidizing methanol and secondary amine DMA to form essential C- and N-based intermediates on different active sites of WO_2 and NiOOH , respectively, followed by a fast C–N coupling process at the $\text{WO}_2\text{--NiOOH}$ interfaces (Figure 1b). Methanol and DMA are economically viable C- and N-source materials that can be obtained through biomass and ammonia-methylation technologies at competitive market prices.^{24,25} Our approach involves incorporating WO_2 into NiOOH to enhance DMA electrooxidation kinetics, where WO_2 enhances DMA oxidation to the $(\text{CH}_3)_2\text{N}^*$ intermediate, and concurrently, methanol is moderately oxidized to an aldehyde intermediate (${}^*\text{CHO}$) on NiOOH . The active interaction between the relatively weakly bonded ${}^*\text{CHO}$ on NiOOH and strongly adsorbed $(\text{CH}_3)_2\text{N}^*$ on nearby WO_2 lowers the overall energy barrier for C–N coupling. Remarkably, the fabricated $\text{WO}_2\text{--NiOOH}/\text{Ni}$ catalyst (*in situ*-formed $\text{WO}_2\text{--NiOOH}$ on Ni) delivered a DMF Faradaic efficiency (FE_{DMF}) of ~50% at 100 mA cm⁻² and a DMF yield rate exceeding 400 $\mu\text{mol cm}^{-2} \text{ h}^{-1}$,

with stability over five consecutive 16 h cycles of operation. At an increased area, 1.4 g of DMF was produced during 3 h of electrolysis on a 15 cm² $\text{WO}_2\text{--NiOOH}/\text{Ni}$ electrode.

In situ infrared spectroscopy (IR) with isotope-labeling experiments, quasi-*in situ* electron paramagnetic resonance (EPR) trapping experiments, and electrochemical operating experiments revealed selective anodic oxidation of methanol and DMA to essential C- and N-intermediates on $\text{WO}_2\text{--NiOOH}/\text{Ni}$ for the consequent thermochemical C–N coupling toward DMF synthesis, following a relay catalysis process. Density functional theory (DFT) calculations confirmed that the strongly and weakly adsorbed $(\text{CH}_3)_2\text{N}^*$ and ${}^*\text{CHO}$ intermediates at the $\text{WO}_2\text{--NiOOH}$ interface reduce the activation energy for C–N coupling, in line with the electrochemical results of the enhanced DMF-synthesis activity with $\text{WO}_2\text{--NiOOH}/\text{Ni}$ catalyst.

RESULTS AND DISCUSSION

We screened a variety of metal catalysts for the electrosynthesis of DMF at a constant current density of 100 mA cm⁻² for 3 h in a three-electrode, membrane-free cell. A 2:1 (v/v) mixture of methanol (99.5%, Macklin) and dimethylamine (40%, Macklin) was used as the reactants, and 0.5 M KHCO₃ was used as the electrolyte. A Pt sheet, an Ag/AgCl electrode, and a metal catalyst were used as the cathode, reference electrode, and anode, respectively. The generated liquid products were analyzed quantitatively by ¹H nuclear magnetic resonance (¹H NMR) spectroscopy (Figure S3). The generated DMF was further validated using high-performance liquid chromatography (HPLC) and liquid chromatography–mass spectrometry (LC–MS) (Figures S4 and S5). Additional experimental details, including electrode fabrication, scanning electron microscopy (SEM) characterization (Figures S6 and S7), and performance evaluation, are provided in the Supporting Information.

Figure 2a shows that, among the examined electrodes, including Co, Fe, Pt, Ni, Pt/Ni, Cr/Ni, Mo/Ni, and W, the W/Ni ($\text{WO}_2\text{--NiOOH}/\text{Ni}$) electrode exhibited the highest catalytic activity for electrocatalytic co-oxidating methanol and DMA to DMF, delivering a Faradaic efficiency (FE) of 47% and a 438 $\mu\text{mol cm}^{-2} \text{ h}^{-1}$ DMF yield at 100 mA cm⁻². This is impressive compared to recently published work on electrosynthesis of other organonitrogen small molecules, such as urea, methylamine, formamide, etc., from C- and N-containing substances (Table S4). Figure 2b shows a distinct ¹H NMR peak at ~7.81 ppm that corresponds to the 1.31 mmol of DMF synthesized on $\text{WO}_2\text{--NiOOH}/\text{Ni}$ during a 3 h reaction at 100 mA cm⁻². Other byproducts, including N-methylformamide, formamide, formate, and formaldehyde, were detected by NMR or ultraviolet–visible (UV–vis) spectroscopy (Figure S8). Overoxidation products such as CO₂, CO, N₂, and NO_x were almost null, falling below the detecting limitation in gas chromatography (GC) analysis during the same period of electrochemical oxidation. Furthermore, $\text{WO}_2\text{--NiOOH}/\text{Ni}$ delivered a higher DMF partial current density across a wide range of applied potentials than the Pt, Ni, and Pt/Ni catalysts (Figure 2c). Remarkably, the DMF partial current density exceeded 50 mA cm⁻² at a relatively low applied potential of ~2 V, consistent with a commercially viable process according to the TEA calculations in Figures S1 and S2. Further details regarding electrodes and performance, including the amount of W loaded on Ni, a performance comparison between *in situ*-formed WO_2 and

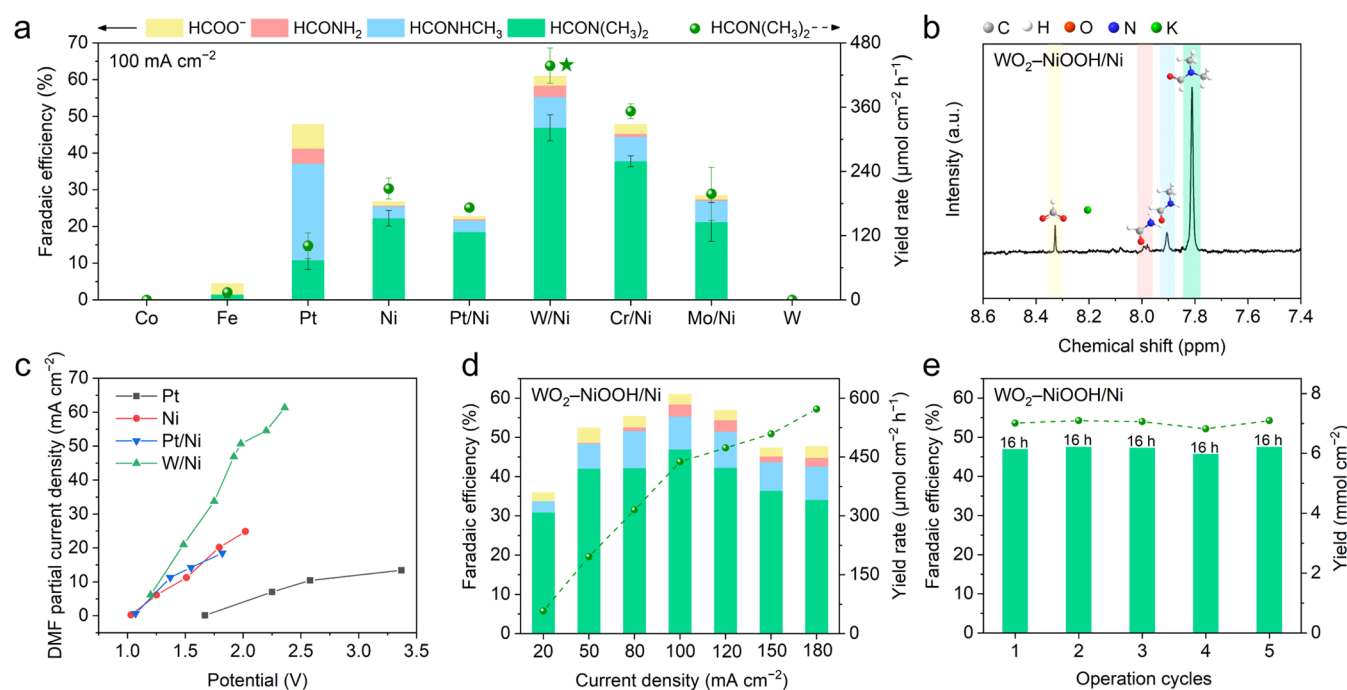


Figure 2. (a) Comparing the DMF-electrosynthesis performance with different catalysts at 100 mA cm^{-2} (asterisk denotes the highest DMF yield rate under $\text{WO}_2\text{-NiOOH/Ni}$ electrocatalysis). (b) Typical ${}^1\text{H}$ NMR spectrum of the carbonaceous liquid products produced by $\text{WO}_2\text{-NiOOH/Ni}$ catalysis. (c) Comparing DMF partial current densities at different applied potentials. (d) DMF-electrosynthesis performance of $\text{WO}_2\text{-NiOOH/Ni}$ at different current densities. (e) Continuous DMF electrosynthesis using $\text{WO}_2\text{-NiOOH/Ni}$ (80 h).

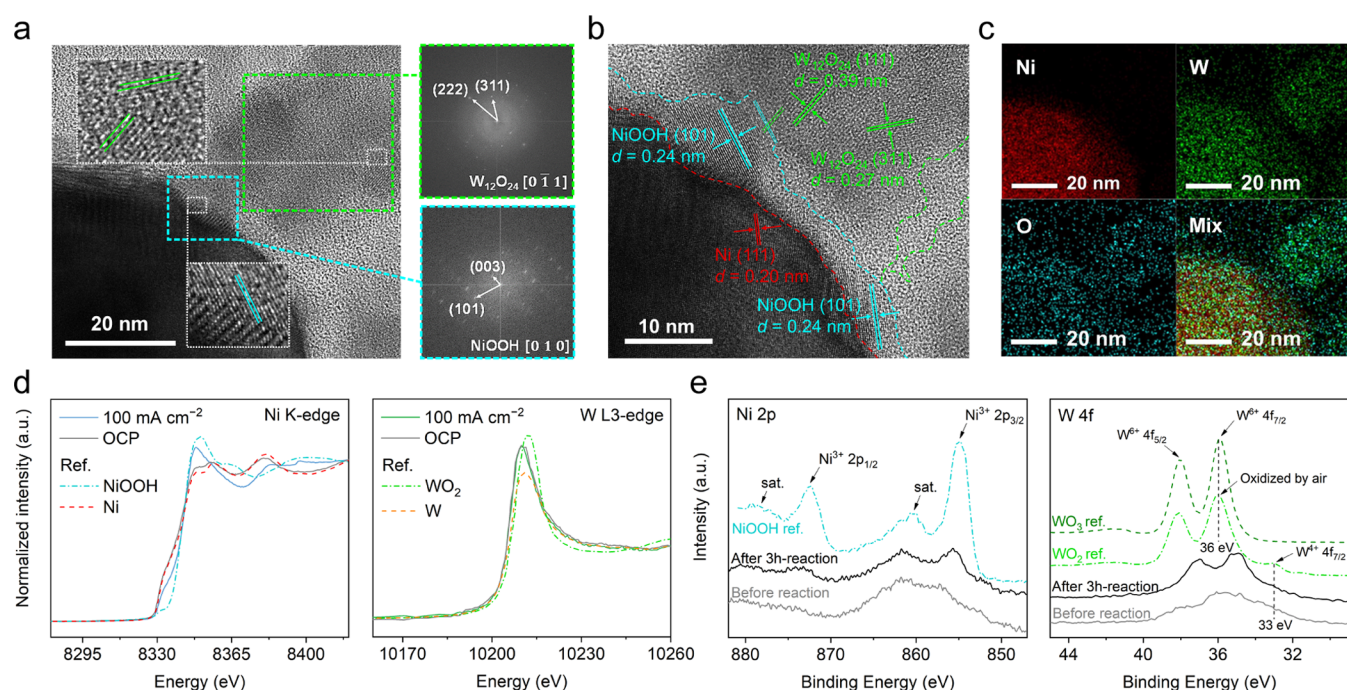


Figure 3. (a) HRTEM image of $\text{WO}_2\text{-NiOOH/Ni}$ and the corresponding fast Fourier-transform patterns. The enlarged magnification of the lattice fringes in the corresponding HRTEM area is presented in the white dashed boxes. (b) HRTEM image of $\text{WO}_2\text{-NiOOH/Ni}$. The red, cyan, and green dashed lines outline the Ni, NiOOH, and $\text{W}_{12}\text{O}_{24}$ lattices, respectively. (c) TEM-EDS maps of $\text{WO}_2\text{-NiOOH/Ni}$. (d) XANES Ni K-edge and W L3-edge spectra of $\text{WO}_2\text{-NiOOH/Ni}$ at the OCP and 100 mA cm^{-2} . (e) Ni 2p and W 4f narrow-scan XPS spectra of $\text{WO}_2\text{-NiOOH/Ni}$ and the reference samples.

loaded WO_2 on Ni, the methanol concentration and methanol-to-dimethylamine volume ratio, and electrolyte pH, are provided in Figures S9–S13.

DMF was stably produced over five consecutive rounds of 16 h electrosynthesis at a constant current density of 100 mA

cm^{-2} (Figures 2d and S14) using the $\text{WO}_2\text{-NiOOH/Ni}$ catalyst and 2:1 (v/v) methanol/DMA in 0.5 M KHCO_3 without any noticeable decrease in FE and yield rate (Figures 2e and S15). This result highlights the durability of the $\text{WO}_2\text{-NiOOH/Ni}$ catalyst. Furthermore, during the anodic DMF-

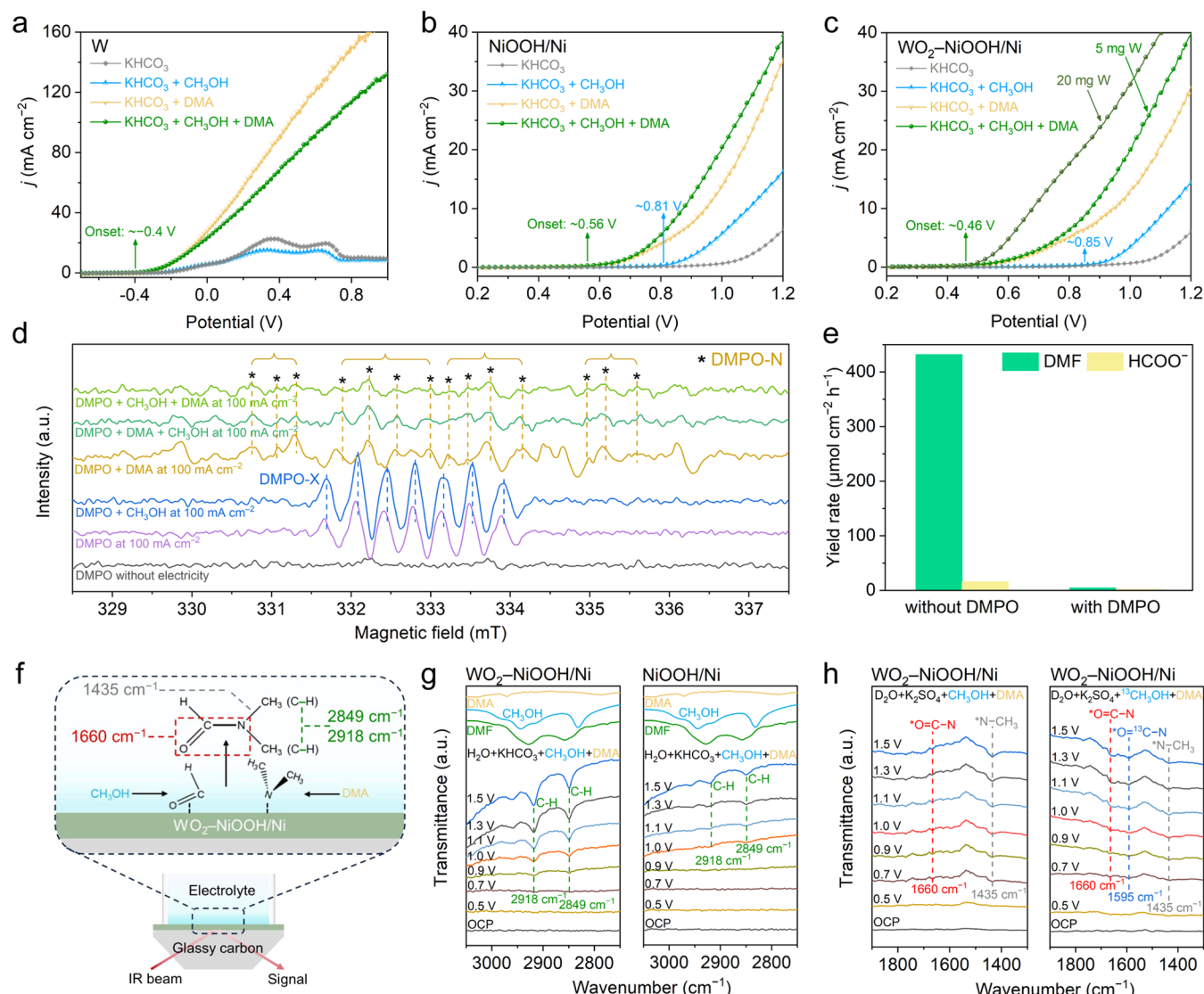


Figure 4. (a–c) LSV traces of W, NiOOH/Ni, and $\text{WO}_2\text{-NiOOH/Ni}$ in electrolytes containing various reactants. (d) Quasi-*in situ* EPR trapping experiments for measuring electrolytes immediately after electrolysis. DMPO was used as the radical trapping agent. * denotes nitrogen radicals. (e) DMF electrosynthesis with and without the presence of 0.2 M DMPO scavenger on $\text{WO}_2\text{-NiOOH/Ni}$ at 100 mA cm^{-2} for 1.5 h. (f) Illustrating the *in situ* ATR-FTIR electrochemical measurement using a $\text{WO}_2\text{-NiOOH/Ni}$ catalyst. (g, h) *In situ* ATR-FTIR spectra of $\text{WO}_2\text{-NiOOH/Ni}$ and NiOOH/Ni.

synthesis process, an equivalent amount of H_2 was produced on the cathode. GC analysis verified ~95% H_2 FE on both 1 cm^2 Ni foam and Pt sheet cathodes during 3 h electrolysis.

Scanning electron microscopy (SEM), energy-dispersive X-ray spectroscopy (EDS), transmission electron microscopy (TEM), X-ray absorption spectroscopy (XAS), X-ray photo-electron spectroscopy (XPS), and X-ray diffraction (XRD) patterns were used to understand the structure and chemical states of the most efficient $\text{WO}_2\text{-NiOOH/Ni}$ catalyst. The SEM images (Figure S17) and the corresponding EDS elemental maps (Figure S18 and Table S1) reveal uniformly mixed W/Ni oxides on Ni metal surfaces; this W/Ni-oxide-on-Ni structure is stable through continuous 16 h electrocatalytic co-oxidation at 100 mA cm^{-2} (Figure S19). The high-resolution TEM (HRTEM) images, fast Fourier-transform (FFT) patterns, and corresponding EDS maps of the postreaction samples confirm the presence of distinctly mixed NiOOH/ WO_2 nanoparticles (identified as $\text{W}_{12}\text{O}_{24}$) on metallic Ni surfaces (Figures 3a,c, and S20). The HRTEM

image in Figure 3b reveals lattice fringes with spacings of 0.20 and 0.24 nm that correspond to the $\text{Ni}(111)$ and $\text{NiOOH}(101)$ crystal planes, respectively, as well as lattice spacings of 0.39 and 0.27 nm that correspond to $\text{W}_{12}\text{O}_{24}(111)$ and $\text{W}_{12}\text{O}_{24}(311)$, respectively. Notably, clear NiOOH/ WO_2 interfaces were observed. These results were further verified by electron diffraction pattern simulations using the ReciPro TEM and FFT pattern simulation software (Figures S21 and S22).

In situ XAS was used to gain further insight into the valence states of the metals during the DMF electrosynthesis at 100 mA cm^{-2} . As shown in Figure 3d, the X-ray absorption near-edge structure (XANES) Ni K-edge signals (obtained after 5 min of electrolysis to reach the electrochemical steady-state conditions) reveal an average Ni valence between Ni^0 and Ni^{3+} . Meanwhile, the W L3-edge white-line intensity was observed to fall between those of commercial W and WO_2 powders, which suggests that Ni is oxidized to NiOOH and W is oxidized to WO_2 during DMF synthesis. The linear combination fitting (LCF) results reveal the presence of

approximately 24.9% NiOOH at the Ni K-edge and 35.9% WO_2 at the W L3-edge (Figure S23).

We used XPS to characterize the surface oxidation states of Ni and W on the $\text{WO}_2\text{--NiOOH}/\text{Ni}$ catalyst before and after a 3 h oxidation reaction; these spectra were also compared with those of laboratory-made NiOOH, commercial WO_2 (Aladdin, 99.9% metal basis), and WO_3 (Macklin, 99.99% metal basis) acquired under identical conditions. As shown in Figure 3e, the postreaction $\text{WO}_2\text{--NiOOH}/\text{Ni}$ catalyst exhibited more intense peaks associated with Ni^{3+} and W^{x+} ($x \geq 4$) species, consistent with the TEM and XAS findings. The narrow-scan O 1s XPS spectra in Figure S24 confirmed the presence of hydroxylated O and oxide species on the catalyst after the electrochemical co-oxidation reaction. XRD patterns confirm the presence of metallic W and Ni in the electrode bulk, which remained unchanged after 16 h of reaction (Figure S25).

To understand the possible reaction pathways involved in the electrosynthesis of DMF and the associated reaction energetics on W, NiOOH/Ni, and $\text{WO}_2\text{--NiOOH}/\text{Ni}$ catalysts, we first conducted linear sweep voltammetry (LSV) studies of electrolytes containing different reactants. Figure 4a,b show that the pure W electrode has a more cathodic onset potential for DMA oxidation than the NiOOH/Ni electrode, consistent with the W surface having a strong N–H bond-activating capability. However, it is worth noting that a large portion of the metallic W electrode had been transformed into WO_x after ~1 h of reaction in a KHCO_3 electrolyte with CH_3OH and DMA. This transformation led to a significant decrease in electrical conductivity, rendering it unsuitable for the co-oxidation reaction (Figure S26). Additionally, we deduced that W exhibited sluggish methanol-oxidation kinetics that is slower than that of the self-oxidation of W based on the LSV data for W in a KHCO_3 electrolyte containing CH_3OH . Conversely, the NiOOH/Ni catalyst exhibited moderate activity for the oxidation of methanol and was stable under oxidative conditions across the pH 8–11 range. Therefore, W-loaded NiOOH/Ni catalysts were developed to electrochemically co-oxidize DMA and methanol. Figure 4b,c show that $\text{WO}_2\text{--NiOOH}/\text{Ni}$ exhibits an earlier onset potential for DMA oxidation (~0.46 V vs Ag/AgCl) than NiOOH/Ni (~0.56 V). Moreover, $\text{WO}_2\text{--NiOOH}/\text{Ni}$ exhibited an onset potential for methanol oxidation of ~0.85 V vs Ag/AgCl, which is slightly delayed but similar to that of NiOOH/Ni (~0.81 V vs Ag/AgCl).

We conducted DFT calculations to examine the oxidation of DMA and methanol on the WO_2 and NiOOH catalysts. As shown in Figure S39, our calculations reveal that the limiting energies for methanol oxidation are 0.83 eV on NiOOH and 0.92 eV on WO_2 . These findings correlate with the LSV curves in Figure 4a,b, where the onset potential for methanol oxidation on NiOOH/Ni is ~0.81 V (Figure 4b). The self-oxidation of W initiates at ~−0.2 V (Figure 4a), which is significantly more cathodic than the DFT-calculated methanol oxidation potential of 0.92 V, indicating that self-oxidation of W is prior to methanol oxidation (Figure 4a). For DMA oxidation, DFT calculations indicate the limiting energies of 0.25 eV on NiOOH and −0.56 eV on WO_2 , which aligns with the experimental LSV curves in Figure 4a,b.

Accordingly, we propose a relay catalysis mechanism based on these observations in which DMA is preferentially oxidized and dehydrogenated to form $(\text{CH}_3)_2\text{N}^*$ intermediate on *in situ*-formed WO_2 nanoparticles while methanol is preferentially oxidized on nearby *in situ*-formed NiOOH to form $^*\text{CHO}$.

Active C–N coupling occurs between the generated $^*\text{CHO}$ and $^*\text{N}(\text{CH}_3)_2$ intermediates at the $\text{WO}_2\text{--NiOOH}$ interface to produce DMF (Figure S27).

To validate the C–N coupling mechanism, we conducted quasi-*in situ* electron paramagnetic resonance (EPR) experiments using 5,5-dimethyl-1-pyrroline N-oxide (DMPO) as the radical trapping agent for capturing N-centered radical species (denoted as *) in the electrolytes right after electrolysis. The schematic in Figure S28 shows the EPR testing procedure. Results reveal new DMPO-trapped N-centered radical signals (DMPO-N) with four sets of multiplets (Figure 4d) observed during both the electrochemical oxidization of DMA alone (yellow curve) and when DMA and methanol were co-oxidized (green curve).²⁶ A detailed comparison between the EPR results in this work and the previous report consolidates DMPO-captured N-radicals generated from DMA oxidation (Figure S29). In contrast, under the same anodic current conditions, only DMPO self-oxidation signals (DMPO-X) were observed in the electrolytes without DMA, in line with the seven-line signals attributed to the self-oxidation of DMPO.²⁷ These results indicate that DMA was oxidized on $\text{WO}_2\text{--NiOOH}$ to generate the $^*\text{N}$ intermediate for the consequent C–N coupling. In addition, further mechanistic analysis indicates that nucleophilic attack of amines on aldehydes is unlikely to occur in our study because the N source DMA is a secondary amine (R_2HN) with only one H atom bonded to the N atom, which cannot support dehydration mechanism that requires at least two H atoms, as typically occurs in ammonia (NH_3) or primary amines (RNH_2) (Figure S30).²⁸ Moreover, DMA also possesses higher steric hindrance that inhibits the nucleophilicity of aldehydes to form a C–N bond compared to ammonia or primary amines.²⁹ These results collectively suggest the C–N coupling mechanism for DMF synthesis in this study. Additionally, *via* electrochemical experiments, we found that the presence of the radical scavenger DMPO during the reaction process inhibited the formation of the product DMF (Figure 4e). This aligns with the previous studies,³⁰ indicating that DMPO can trap N-centered radicals, thereby inhibiting the subsequent $^*\text{C}\text{--}^*\text{N}$ coupling.

In situ attenuated total reflection flourier transformed infrared (ATR-FTIR) spectroscopy with isotope-labeling experiments was conducted to verify the improved DMF production on the $\text{WO}_2\text{--NiOOH}/\text{Ni}$ electrode (Figure 4f). Figure 4g shows two distinct C–H stretching vibrations (green dashed line) ascribable to DMF at ~2850 and ~2920 cm^{-1} at 0.7 V vs Ag/AgCl on $\text{WO}_2\text{--NiOOH}/\text{Ni}$. These peaks became more intense with increasing applied potential, consistent with the production of more DMF. In contrast, these C–H stretching peaks appeared at a much higher potential (above 1.0 V vs Ag/AgCl) on NiOOH/Ni. Importantly, under potentials greater than 0.7 V vs Ag/AgCl, we observed a characteristic peak at ~1660 cm^{-1} corresponding to the $\text{O}=\text{C}$ bond stretching in $^*\text{O}=\text{C}\text{--}\text{N}$ in the DMF (Figure S31a).^{31,32} We then switched the electrolyte to 0.5 M K_2SO_4 in deuterium oxide (D_2O) to eliminate interference from the H_2O signal at ~1635 cm^{-1} and the carbonate signal at ~1380 cm^{-1} . Figure 4h shows that the $^*\text{O}=\text{C}\text{--}\text{N}$ (red dashed line) in DMF appeared at ~0.7 V vs Ag/AgCl for $\text{WO}_2\text{--NiOOH}/\text{Ni}$. *In situ* ATR-FTIR using ^{13}C -labeled methanol revealed an isotopic effect that caused an additional $^*\text{O}=\text{C}\text{--}^{13}\text{C}\text{--}\text{N}$ signal at ~1595 cm^{-1} (blue dashed line in Figure 4h), which shifted to lower wavenumbers beneath the $^*\text{O}=\text{C}\text{--}^{12}\text{C}\text{--}\text{N}$ signal.³³ Control

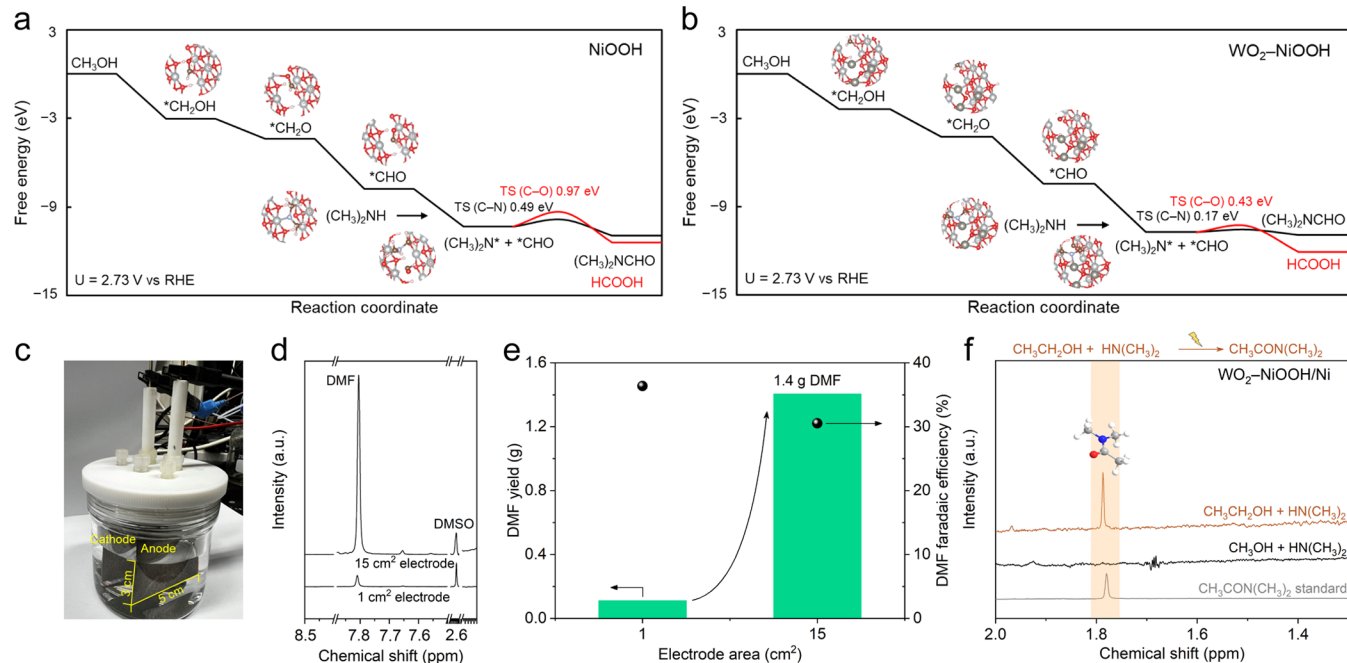


Figure 5. (a, b) Free-energy diagrams for $(\text{CH}_3)_2\text{NCHO}$ formation over NiOOH and WO₂-NiOOH. (c) Schematic illustration of a 15 cm² WO₂-NiOOH/Ni anode and a 15 cm² Ni foam cathode for electrosynthesis of DMF. (d) ¹H NMR spectra of the carbonaceous liquid products produced by 15 and 1 cm² WO₂-NiOOH/Ni catalysis at 150 mA cm⁻² for 3 h. (e) DMF yield and FE over 1 and 15 cm² WO₂-NiOOH/Ni electrode at 150 mA cm⁻² for 3 h. (f) Detection of *N,N*-dimethylacetamide by ¹H NMR spectroscopy as an extendable product.

experiments confirmed the absence of signals in the range from 1590 to 1660 cm⁻¹ during the electrooxidation of ¹³C-labeled methanol and the co-oxidation of ¹²C-methanol and NH₃ (Figure S31b,c). These results collectively suggest that the *O= ¹²C-N (~1660 cm⁻¹) and *O= ¹³C-N (~1595 cm⁻¹) vibration signals originate from DMF after C–N coupling.

In addition, we found that the N–C vibrations in DMF at ~1435 cm⁻¹ did not shift during the coelectrooxidation of ¹³C-labeled methanol and DMA, suggesting that this signal may be attributed to *N–CH₃ (gray dashed line) in DMF. This *N–CH₃ signal at ~1435 cm⁻¹ appears at ~0.7 V vs Ag/AgCl for WO₂-NiOOH/Ni (after subtracting the background DMA C–N signal), which is lower than the ~1.0 V vs Ag/AgCl recorded for NiOOH/Ni (Figure S31d).

We used DFT simulations to delve more deeply into the energy barrier associated with the catalytic co-oxidation of WO₂-NiOOH (Figure 5a) and pure NiOOH (Figure 5b); computational methods are provided in Section 3 of the Supporting Information. In NiOOH, both C (associated with methanol oxidation) and N (associated with DMA oxidation) species were activated at the Ni sites; in WO₂-NiOOH, at the interface between WO₂ and NiOOH, the C species were activated at the Ni sites, while the N species tended to be activated at the W sites. The computational models are illustrated in Figures S37 and S38; solvent effects were corrected for conducting the calculations as all adsorbates are stabilized through a H bond with water, as detailed in Table S5 of the Supporting Information. Electrooxidative dehydrogenation proceeds easily with a significant decrease in free energy at a working potential of 1.92 V vs Ag/AgCl (2.73 V vs RHE). The activity and selectivity for DMF production primarily depend on the barriers associated with the formation of C–N and C–O bonds. The calculations suggest that C–N coupling has a barrier of 0.49 eV, which is lower than that (0.97 eV) for the formation of the C–O bond, indicative of C–N selectivity.

The introduction of WO₂ leads to the W site (-3.29 eV) becoming more favorable than the Ni site (-2.53 eV) for activating N species and forming the $(\text{CH}_3)_2\text{N}^*$ intermediate, which facilitates the subsequent C–N coupling reaction. The projected density of states (PDOS) results (Figure S40) further confirm that the addition of WO₂ to NiOOH strengthens the resonant regions of the Ni 3d and N 2p bonding orbitals, especially at positions around -7 eV (black arrow), suggestive of enhanced N activation and the stronger adsorption of N-related species. The Ni sites adsorb *CHO more weakly at the WO₂-NiOOH interface, which further promotes C–N coupling over C–O bond formation. These findings are corroborated by the PDOS results (Figure S41), which show that the resonance regions of the Ni 3d and C 2p bonding orbitals are significantly weakened by adding WO₂ to NiOOH. The C 2p orbital shifted further from the Fermi level, consistent with a lower level of activation and the weaker adsorption of C species. Consequently, the activation energy associated with *CHO/ $(\text{CH}_3)_2\text{N}^*$ coupling to form a C–N bond is significantly lower (only 0.17 eV) on the WO₂-NiOOH catalyst, which facilitates high-performance DMF electrosynthesis on WO₂-NiOOH/Ni. Importantly, while the more weakly adsorbed *CHO can potentially facilitate C–O bond formation, the energy barrier for this process is 0.43 eV, which is much higher than that of 0.17 eV for C–N coupling, suggesting that the WO₂-NiOOH/Ni catalyst offers both high selectivity and activity for C–N coupling products.

The DFT calculations showed that the formation of the *CHO intermediate plays a crucial role in the C–N coupling reaction that yields DMF. We conducted online differential electrochemical mass spectrometry (DEMS) analysis during the coelectrooxidation of DMA and methanol on WO₂-NiOOH/Ni; signals of formaldehyde intermediates appeared at a positive electrode potential of 1.2 V (Figure S32). To further verify the importance of the formation of *CHO during

C–N coupling, we conducted a series of control experiments using $\text{WO}_2\text{--NiOOH/Ni}$. We initially changed the C source from methanol to formaldehyde or formate with other reaction conditions unchanged. A DMF yield rate of $\sim 300 \mu\text{mol cm}^{-2} \text{ h}^{-1}$ was obtained when formaldehyde and DMA were co-oxidized (Table S2). However, a much lower yield rate of $\sim 26 \mu\text{mol cm}^{-2} \text{ h}^{-1}$ was obtained when formate and DMA were co-oxidized (the comparison of ^1H NMR spectra is shown in Figure S34). The limited DMF production observed in the latter case is due to the fact that formate is a subsequent oxidation product of methanol or formaldehyde and cannot form a sufficient *CHO intermediate for synthesizing DMF under electrooxidation conditions (Figure S35). In addition, no DMF generation was observed at the cathode during the anodic electrochemical oxidation of methanol and DMA in an H-type cell with a Nafion membrane separating the anolyte and catholyte (Figure S36). Finally, we electrooxidized pure methanol in the absence of a N source. In this case, only a small amount of HCOO^- ($14 \mu\text{mol cm}^{-2} \text{ h}^{-1}$) was detected in the liquid-phase product after 3 h of electrolysis, with no amide-like substances formed, which indicates that methanol is progressively oxidized to formaldehyde, HCOO^- , CO, and CO_2 in the absence of N species (Table S3). Collectively, these results suggest that *CHO and $^*\text{N}(\text{CH}_3)_2$ are critical intermediates required in the C–N coupling step and, consequently, the formation of DMF.

We fabricated an enlarged $\text{WO}_2\text{--NiOOH/Ni}$ anode ($5 \times 3 \text{ cm}^2$) for DMF production in a 0.5 M KHCO_3 electrolyte (Figure 5c). During a 3 h coelectrolysis of DMA and methanol at a constant current density of 150 mA cm^{-2} , 1.4 g of DMF was produced, with a notable 30% DMF FE (Figure 5d,e). To validate the feasibility of the C–N coupling mechanism in the extension of synthesizing other amides, we present the successful electrosynthesis of *N,N*-dimethylacetamide by coelectrooxidizing ethanol and DMA on $\text{WO}_2\text{--NiOOH/Ni}$ (Figure 5f).

CONCLUSIONS

We designed a relay catalysis route for the selective and sustainable electrosynthesis of DMF from methanol and dimethylamine on a robust $\text{WO}_2\text{--NiOOH-on-Ni}$ catalyst under ambient conditions. Electrochemical experiments and DFT calculations were used to show that WO_2 promotes DMA oxidation on its surface through relatively strong binding to $(\text{CH}_3)_2\text{N}^*$, while NiOOH facilitates methanol oxidation and the formation of relatively weakly bound *CHO. This strong/weak intermediate binding at the WO_2/NiOOH interface efficiently reduces the energy required for the C–N coupling step, thereby promoting the electrochemical synthesis of DMF. *In situ* ATR-FTIR spectroscopy with isotope-labeling experiments, quasi-*in situ* EPR trapping experiments, online DEMS analysis, and electrochemical operating experiments confirmed C–N bond formation and the enhanced activity for DMF synthesis on the $\text{WO}_2\text{--NiOOH/Ni}$ catalyst. TEM and *in situ* XAS confirmed the existence of a stable $\text{WO}_2\text{--NiOOH/Ni}$ structure that enables active DMF electrosynthesis with a DMF FE of $\sim 50\%$ and a DMF yield rate exceeding $400 \mu\text{mol cm}^{-2} \text{ h}^{-1}$ at a current density of 100 mA cm^{-2} over 80 h. To showcase the scalability of the electrosynthesis, 1.4 g of DMF was produced on a 15 cm^2 $\text{WO}_2\text{--NiOOH/Ni}$ electrode over a 3 h electrolysis period. This study demonstrated the effectiveness of catalyst and catalytic reaction pathway design

for the sustainable electrified synthesis of high-value organic chemicals.

ASSOCIATED CONTENT

Supporting Information

The Supporting Information is available free of charge at <https://pubs.acs.org/doi/10.1021/jacs.4c07142>.

Experimental procedures, additional results and discussion, and computational methods (PDF)

AUTHOR INFORMATION

Corresponding Authors

Miao Zhong – College of Engineering and Applied Sciences, Collaborative Innovation Centre of Advanced Microstructures, National Laboratory of Solid State Microstructures, Frontiers Science Center for Critical Earth Material Cycling, Nanjing University, Nanjing 210023, China;  orcid.org/0000-0002-1253-7783; Email: miaozhong@nju.edu.cn

Haoshen Zhou – College of Engineering and Applied Sciences, Collaborative Innovation Centre of Advanced Microstructures, National Laboratory of Solid State Microstructures, Frontiers Science Center for Critical Earth Material Cycling, Nanjing University, Nanjing 210023, China;  orcid.org/0000-0001-8112-3739; Email: hszhou@nju.edu.cn

Authors

Weihang Li – College of Engineering and Applied Sciences, Collaborative Innovation Centre of Advanced Microstructures, National Laboratory of Solid State Microstructures, Frontiers Science Center for Critical Earth Material Cycling, Nanjing University, Nanjing 210023, China

Haoyang Jiang – College of Engineering and Applied Sciences, Collaborative Innovation Centre of Advanced Microstructures, National Laboratory of Solid State Microstructures, Frontiers Science Center for Critical Earth Material Cycling, Nanjing University, Nanjing 210023, China

Xiang Zhang – College of Engineering and Applied Sciences, Collaborative Innovation Centre of Advanced Microstructures, National Laboratory of Solid State Microstructures, Frontiers Science Center for Critical Earth Material Cycling, Nanjing University, Nanjing 210023, China

Bo Lei – College of Engineering and Applied Sciences, Collaborative Innovation Centre of Advanced Microstructures, National Laboratory of Solid State Microstructures, Frontiers Science Center for Critical Earth Material Cycling, Nanjing University, Nanjing 210023, China

Le Li – College of Engineering and Applied Sciences, Collaborative Innovation Centre of Advanced Microstructures, National Laboratory of Solid State Microstructures, Frontiers Science Center for Critical Earth Material Cycling, Nanjing University, Nanjing 210023, China

Complete contact information is available at:

<https://pubs.acs.org/10.1021/jacs.4c07142>

Author Contributions

The manuscript was written through contributions of all authors. All authors have given approval to the final version of the manuscript.

Notes

The authors declare no competing financial interest.

ACKNOWLEDGMENTS

This work was financially supported by the National Natural Science Foundation of China (grant number 22272078), the National Key R&D Program of China (No. 2020YFA0406102), and the “Innovation and Entrepreneurship of Talents plan” of Jiangsu Province. We thank Lirong Zheng (Institute of High Energy Physics, Chinese Academy of Sciences) for his help in the XAS test. We thank Chenxi Guo for his valuable discussion in the DFT calculations.

REFERENCES

- (1) Pastoriza-Santos, I.; Liz-Marzán, L. M. *N,N*-Dimethylformamide as a Reaction Medium for Metal Nanoparticle Synthesis. *Adv. Funct. Mater.* **2009**, *19* (5), 679–688.
- (2) Muzart, J. *N,N*-Dimethylformamide: Much More than a Solvent. *Tetrahedron* **2009**, *65* (40), 8313–8323.
- (3) Ding, S.; Jiao, N. *N,N*-Dimethylformamide: A Multipurpose Building Block. *Angew. Chem., Int. Ed.* **2012**, *51* (37), 9226–9237.
- (4) Dimethylformamide (DMF) Market by Type (Reactant and Feedstock), End-use industries (Chemicals, Electronics, Pharmaceutical, and Agrochemical), and Region (Asia Pacific, Europe, North America, Europe, MEA and South America) - Global Forecast to 2027; CH 5950; MarketsandMarkets. 2022.
- (5) Wittcoff, H. A.; Reuben, B. G.; Plotkin, J. S. *Industrial Organic Chemicals*, 3rd ed.; John Wiley and Sons Ltd, 2012; p 506.
- (6) Shen, Y.; Zheng, Q.; Chen, Z. N.; Wen, D.; Clark, J. H.; Xu, X.; Tu, T. Highly Efficient and Selective *N*-Formylation of Amines with CO₂ and H₂ Catalyzed by Porous Organometallic Polymers. *Angew. Chem., Int. Ed.* **2021**, *60* (8), 4125–4132.
- (7) Jacquet, O.; Gomes, C. D. N.; Ephritikhine, M.; Cantat, T. Recycling of Carbon and Silicon Wastes: Room Temperature Formylation of N–H Bonds Using Carbon Dioxide and Poly-methylhydrosiloxane. *J. Am. Chem. Soc.* **2012**, *134* (6), 2934–2937.
- (8) Aragonès, A. C.; Haworth, N. L.; Darwish, N.; Ciampi, S.; Bloomfield, N. J.; Wallace, G. G.; Diez-Perez, I.; Coote, M. L. Electrostatic Catalysis of a Diels–Alder Reaction. *Nature* **2016**, *531* (7592), 88–91.
- (9) Guo, C.; Zhou, W.; Lan, X.; Wang, Y.; Li, T.; Han, S.; Yu, Y.; Zhang, B. Electrochemical Upgrading of Formic Acid to Formamide via Coupling Nitrite Co-Reduction. *J. Am. Chem. Soc.* **2022**, *144* (35), 16006–16011.
- (10) Peng, X.; Zeng, L.; Wang, D.; Liu, Z.; Li, Y.; Li, Z.; Yang, B.; Lei, L.; Dai, L.; Hou, Y. Electrochemical C–N Coupling of CO₂ and Nitrogenous Small Molecules for the Electrosynthesis of Organonitrogen Compounds. *Chem. Soc. Rev.* **2023**, *52*, 2193–2237.
- (11) Pople, J. M. M.; Nicholls, T. P.; Pham, L. N.; Bloch, W. M.; Lisboa, L. S.; Perkins, M. V.; Gibson, C. T.; Coote, M. L.; Jia, Z.; Chalker, J. M. Electrochemical Synthesis of Poly(trisulfides). *J. Am. Chem. Soc.* **2023**, *145* (21), 11798–11810.
- (12) Lv, C.; Zhong, L.; Liu, H.; Fang, Z.; Yan, C.; Chen, M.; Kong, Y.; Lee, C.; Liu, D.; Li, S.; Liu, J.; Song, L.; Chen, G.; Yan, Q.; Yu, G. Selective Electrocatalytic Synthesis of Urea with Nitrate and Carbon Dioxide. *Nat. Sustainability* **2021**, *4* (10), 868–876.
- (13) Yuan, M.; Chen, J.; Bai, Y.; Liu, Z.; Zhang, J.; Zhao, T.; Wang, Q.; Li, S.; He, H.; Zhang, G. Unveiling Electrochemical Urea Synthesis by Co-Activation of CO₂ and N₂ with Mott–Schottky Heterostructure Catalysts. *Angew. Chem., Int. Ed.* **2021**, *60* (19), 10910–10918.
- (14) Lv, C.; Lee, C.; Zhong, L.; Liu, H.; Liu, J.; Yang, L.; Yan, C.; Yu, W.; Hng, H. H.; Qi, Z.; Song, L.; Li, S.; Loh, K. P.; Yan, Q.; Yu, G. A Defect Engineered Electrocatalyst that Promotes High-Efficiency Urea Synthesis under Ambient Conditions. *ACS Nano* **2022**, *16* (5), 8213–8222.
- (15) Wei, X.; Wen, X.; Liu, Y.; Chen, C.; Xie, C.; Wang, D.; Qiu, M.; He, N.; Zhou, P.; Chen, W.; Cheng, J.; Lin, H.; Jia, J.; Fu, X. Z.; Wang, S. Oxygen Vacancy-Mediated Selective C–N Coupling toward Electrocatalytic Urea Synthesis. *J. Am. Chem. Soc.* **2022**, *144* (26), 11530–11535.
- (16) Zhao, Y.; Ding, Y.; Li, W.; Liu, C.; Li, Y.; Zhao, Z.; Shan, Y.; Li, F.; Sun, L.; Li, F. Efficient Urea Electrosynthesis from Carbon Dioxide and Nitrate via Alternating Cu–W Bimetallic C–N Coupling Sites. *Nat. Commun.* **2023**, *14* (1), No. 4491.
- (17) Wu, Y.; Jiang, Z.; Lin, Z.; Liang, Y.; Wang, H. Direct Electrosynthesis of Methylamine from Carbon Dioxide and Nitrate. *Nat. Sustainability* **2021**, *4* (8), 725–730.
- (18) Meng, N.; Shao, J.; Li, H.; Wang, Y.; Fu, X.; Liu, C.; Yu, Y.; Zhang, B. Electrosynthesis of Formamide from Methanol and Ammonia under Ambient Conditions. *Nat. Commun.* **2022**, *13* (1), No. 5452.
- (19) Zhu, J.; Hu, L.; Zhao, P.; Lee, L. Y. S.; Wong, K. Y. Recent Advances in Electrocatalytic Hydrogen Evolution Using Nanoparticles. *Chem. Rev.* **2020**, *120* (2), 851–918.
- (20) Li, L.; Ozden, A.; Guo, S.; de Arquer, F. P. G.; Wang, C.; Zhang, M.; Zhang, J.; Jiang, H.; Wang, W.; Dong, H.; Sinton, D.; Sargent, E. H.; Zhong, M. Stable, Active CO₂ Reduction to Formate via Redox-modulated Stabilization of Active Sites. *Nat. Commun.* **2021**, *12* (1), No. 5223.
- (21) Shafaat, H. S.; Yang, J. Y. Uniting Biological and Chemical Strategies for Selective CO₂ Reduction. *Nat. Catal.* **2021**, *4* (11), 928–933.
- (22) Zhang, J.; Guo, C.; Fang, S.; Zhao, X.; Li, L.; Jiang, H.; Liu, Z.; Fan, Z.; Xu, W.; Xiao, J.; Zhong, M. Accelerating Electrochemical CO₂ Reduction to Multi-carbon Products via Asymmetric Intermediate Binding at Confined Nanointerfaces. *Nat. Commun.* **2023**, *14* (1), No. 1298.
- (23) Shao, J.; Meng, N.; Wang, Y.; Zhang, B.; Yang, K.; Liu, C.; Yu, Y.; Zhang, B. Scalable Electrosynthesis of Formamide through C–N Coupling at the Industrially Relevant Current Density of 120 mA cm⁻². *Angew. Chem., Int. Ed.* **2022**, *61* (44), No. e202213009.
- (24) Vispute, T. P.; Zhang, H.; Sanna, A.; Xiao, R.; Huber, G. W. Renewable Chemical Commodity Feedstocks from Integrated Catalytic Processing of Pyrolysis Oils. *Science* **2010**, *330*, 1222–1227.
- (25) Hayes, K. Industrial Processes for Manufacturing Amines. *Appl. Catal., A* **2001**, *221* (1–2), 187–195.
- (26) Ma, C.-R.; Huang, G.-W.; Xu, H.; Wang, Z.-L.; Li, Z.-H.; Liu, J.; Yang, Y.; Li, G.; Dang, Y.; Wang, F. Site-selective Arene C–H Amination with Iron-aminyl Radical. *Nat. Catal.* **2024**, *7*, 636–645.
- (27) Chen, S.; Hu, J.; Lu, L.; Wu, L. Z.; Liang, Z. Q.; Tang, J.; Hou, H.; Liang, S.; Yang, J. Iron Porphyrin-TiO₂ Modulated Peroxymonosulfate Activation for Efficient Degradation of 2,4,6-trichlorophenol with High-valent Iron-oxo Species. *Chemosphere* **2022**, *309*, No. 136744.
- (28) Yamaguchi, K.; Kobayashi, H.; Oishi, T.; Mizuno, N. Heterogeneously Catalyzed Synthesis of Primary Amides Directly from Primary Alcohols and Aqueous Ammonia. *Angew. Chem., Int. Ed.* **2012**, *51* (2), 544–547.
- (29) Gunanathan, C.; Ben-David, Y.; Milstein, D. Direct Synthesis of Amides from Alcohols and Amines with Liberation of H₂. *Science* **2007**, *317* (5839), 790–792.
- (30) Liu, W.; Wang, Y.; Huang, H.; Wang, J.; He, G.; Feng, J.; Yu, T.; Li, Z.; Zou, Z. Spatial Decoupling of Redox Chemistry for Efficient and Highly Selective Amine Photoconversion to Imines. *J. Am. Chem. Soc.* **2023**, *145* (13), 7181–7189.
- (31) Fan, Y.; Liu, T.; Yan, Y.; Xia, Z.; Lu, Y.; Pan, Y.; Wang, R.; Xie, D.; Zhu, Z.; Nga, T. T. T.; Dong, C.-L.; Jing, Y.; Li, Y.; Wang, S.; Zou, Y. Electrochemical Synthesis of Formamide by C–N Coupling with Amine and CO₂ with a High Faradaic Efficiency of 37.5%. *Chem* **2024**, *10*, 1–13.

(32) Jin, M.; Li, A.-Z.; Wang, Y.; Li, J.; Zhou, H.; Li, B.-J.; Duan, H. Electrosynthesis of *N,N*-dimethylformamide from Market-surplus Trimethylamine Coupled with Hydrogen Production. *Green Chem.* **2023**, *25*, 5936–5944.

(33) Chen, C.; Zhu, X.; Wen, X.; Zhou, Y.; Zhou, L.; Li, H.; Tao, L.; Li, Q.; Du, S.; Liu, T.; Yan, D.; Xie, C.; Zou, Y.; Wang, Y.; Chen, R.; Huo, J.; Li, Y.; Cheng, J.; Su, H.; Zhao, X.; Cheng, W.; Liu, Q.; Lin, H.; Luo, J.; Chen, J.; Dong, M.; Cheng, K.; Li, C.; Wang, S. Coupling N₂ and CO₂ in H₂O to synthesize urea under ambient conditions. *Nat. Chem.* **2020**, *12* (8), 717–724.



CAS BIOFINDER DISCOVERY PLATFORM™

BRIDGE BIOLOGY AND CHEMISTRY FOR FASTER ANSWERS

Analyze target relationships,
compound effects, and disease
pathways

Explore the platform

